

Selective Fabrication of Monolayer $1H$ - and $1T'$ - WTe_2

Ryuichi Ando¹, Katsuaki Sugawara^{1,2,3,*}, Tappei Kawakami¹, Takashi Takahashi¹, and Takafumi Sato^{1,2,4,5,6,*}

¹ *Department of Physics, Graduate School of Science, Tohoku University, Sendai 980-8578, Japan*

² *Advanced Institute for Materials Research (WPI-AIMR), Tohoku University, Sendai 980-8577, Japan*

³ *Precursory Research for Embryonic Science and Technology (PRESTO), Japan Science and Technology Agency (JST), Tokyo 102-0076, Japan*

⁴ *Center for Science and Innovation in Spintronics (CSIS), Tohoku University, Sendai 980-8577, Japan*

⁵ *International Center for Synchrotron Radiation Innovation Smart (SRIS), Tohoku University, Sendai 980-8577, Japan*

⁶ *Mathematical Science Center for Co-creative Society (MathCCS), Tohoku University, Sendai 980-8578, Japan*

We selectively fabricated monolayers of octahedral ($1H$) and distorted trigonal ($1T'$) WTe_2 on graphene/SiC(0001) by controlling the substrate temperature during epitaxy. Angle-resolved photoemission spectroscopy, combined with first-principles band-structure calculations, has revealed several drastic differences between these two polymorphs. The $1T'$ phase exhibits a semiconducting character with a nearly-zero energy gap, while the $1H$ phase shows a large band gap and the band splitting at the K/K' point. The present results pave a pathway toward developing nanoelectronic devices based with WTe_2 .

Layered transition metal dichalcogenides (TMDs) exhibit a variety of novel quantum phenomena such as superconductivity, charge-density wave, and metal-insulator transition, depending on the constituent element and the crystal symmetry.¹⁾ TMDs generally take two different types of stable structures; one is $2H$ with a triangular prismatic structure stacked with a two-fold periodicity, and the other is $1T$ with an octahedral structure. It is also known that bulk TMDs containing the group-VI transition metal such as Mo and W take some additional crystal structures different from $2H$ and $1T$ when the growth condition is well controlled. This is highlighted by realization of $1T'$ - $MoTe_2$ upon local heating of bulk $2H$ - $MoTe_2$ crystal, leading to an ohmic homojunction with a very high mobility.²⁾

Here we focus on WTe_2 having two stable structures in bulk, $2H$ and T_d .³⁾ The latter takes

an orthorhombic structure with distorted octahedral $1T'$ layers stacked alternately with 180° rotation.⁴⁾ Bulk $2H\text{-WTe}_2$ is an indirect semiconductor⁵⁾ whereas the monolayer counterpart ($1H$) is predicted to be a direct-gap semiconductor with a spin-split band structure at the K/K' point in the Brillouin zone (BZ) due to the strong spin-orbit coupling (SOC) and the space-inversion-symmetry (SIS) breaking.⁶⁾ The SIS breaking in monolayer $1H$ phase is known to play an essential role in realizing various exotic properties such as circular-light-polarization-dependent photoluminescence⁷⁾ and Ising superconductivity⁸⁾ in pristine monolayer and carrier-doped monolayer $1H\text{-MoS}_2$, respectively. On the other hand, bulk $T_d\text{-WTe}_2$ is a Weyl semimetal with surface Fermi-arc states,^{9,10)} whereas the monolayer counterpart ($1T'\text{-WTe}_2$) is a candidate of two-dimensional topological insulator (2D TI),¹¹⁾ as supported by the observation of edge states in the transport and scanning-tunneling-microscopy (STM) measurements.^{12,13)} While it is important to establish a method to selectively fabricate various crystal phases in order to further functionalize the W-based TMDs, this has yet to be established for monolayer WTe_2 .

In this work, we have succeeded in selectively fabricating $1H$ and $1T'$ monolayers of WTe_2 by precisely controlling the substrate temperature (T_s) during the molecular-beam epitaxy (MBE), and characterized the band structure using ARPES and DFT (density-functional-theory) calculations.

Monolayer WTe_2 was grown on bilayer graphene.¹⁴⁻¹⁶⁾ At first, bilayer graphene was fabricated by resistive heating of an n -type $4H\text{-SiC}(0001)$ single-crystal wafer at 1100°C for 15 min under high vacuum better than 1.0×10^{-9} Torr. Subsequently, a monolayer WTe_2 film was grown by evaporating W atoms on the bilayer graphene substrate in Te-rich atmosphere. We optimized the growth condition by systematically changing T_s during the epitaxial growth, and found that the optimum T_s value to grow $1H$ and $1T'$ films is 280°C and 310°C , respectively [see Fig. 1(a)]. To improve the crystallinity, as-grown monolayer WTe_2 films were annealed for 30 min at the same T_s . *In-situ* ARPES measurements were carried out using an MBS-A1 electron analyzer with a He discharge lamp (photon energy $h\nu = 21.218$ eV) at Tohoku University and a DA-30 electron analyzer (Omicron-Scienta) at beamline BL-28A in Photon Factory, KEK. The energy and angular resolutions were set to be 16 meV and 0.2° , respectively. DFT calculations were carried out by using the QUANTUM-ESPRESSO package¹⁷⁾ with generalized gradient approximation¹⁸⁾ and also with Heyd-Scuseria-Ernzerhof (HSE06) hybrid functional. The plane-wave cutoff energy and uniform k -point mesh were set to be 60 Ry and $10 \times 5 \times 1$, respectively. The thickness of inserted vacuum layer was more than 10 \AA to prevent interlayer interaction. SOC was included in the calculation.

We show in Fig. 1(b) the plot of ARPES intensity at $T = 40$ K for monolayer WTe_2 fabricated

at $T_s = 280$ °C, measured along the Γ K cut of graphene BZ. Figure 1(d) shows the corresponding energy distribution curve (EDC) at the Γ point. One can recognize several key features such as (i) suppression of ARPES intensity in the binding-energy (E_B) range of Fermi level (E_F)-0.5 eV indicative of the semiconducting nature, (ii) a hole band topped at $E_B \sim 1.3$ eV at the Γ point which rapidly moves toward higher E_B on moving away from the Γ point, and (iii) broad intensity at $E_B \sim 0.5$ -1 eV around the K point. These key features are reproduced well in the DFT calculations including SOC for free-standing monolayer $1H$ -WTe₂ (red curves), suggesting that the monolayer fabricated at $T_s = 280$ °C has the $1H$ phase. On the other hand, in the monolayer fabricated at $T_s = 310$ °C [Fig. 1(c, e)], one can identify an obvious difference; four hole bands topped at $E_B \sim 0.1, 0.6, 0.8,$ and 1.3 eV are observed at the Γ point. They are reasonably reproduced by the DFT calculations with HSE06 (red curves) for free-standing monolayer $1T'$ -WTe₂, consistent with the previous study¹⁵⁾ (note that the temperature evolution of the band structure in the $1T'$ phase is reported in a separate work¹⁶⁾). These results indicate that monolayer $1H$ and $1T'$ -WTe₂ phases can be selectively fabricated by fine-tuning T_s during the MBE growth. This conclusion is supported by the Te $4d$ core-level spectrum. While each Te $4d_{3/2}$ and $4d_{5/2}$ spin-orbit satellite is composed of a single peak in the $1H$ phase [see Fig. 1(f)], a two-peaked structure is identified for the $1T'$ phase [Fig. 1(g)]. This is because the $1H$ phase has a single W-Te bond length whereas the $1T'$ phase has two types of bond lengths due to the distorted structure¹⁹⁾, as shown in Fig. 1(a). It is noted here that the electron diffraction experiment does not work well to distinguish the two-fold-symmetric $1T'$ phase because of the inevitable mixture of three domains rotated by 120° from each other due to symmetry mismatch with the graphene substrate with six-fold symmetry, as reported in $1T'$ -WTe₂¹⁵⁾ and other TMDs¹⁹⁾. To resolve the band structure of each domain, nano-ARPES measurement is necessary.

Now we examine the band structure of $1H$ phase in more detail. It is theoretically predicted that the band structure of $1H$ phase shows a spin-valley coupling at the K/K' point [inset to Fig. 2(a)],^{6,14)} causing the spin splitting due to the SIS breaking and the strong SOC. We show in Fig. 2(a) the second-derivative intensity of ARPES spectrum, compared with the DFT calculation at $E_B = 0.4$ -1.7 eV where the band splitting is expected to occur around the K/K' point. In the DFT calculation, we identify the spin-split partners topped at $E_B = 0.7$ and 1.2 eV, respectively, which look to show a reasonable agreement with the experiment despite the broad ARPES intensity. To further examine the band splitting, we show in Fig. 2(b) the energy distribution curve (EDC) at the K point. The EDC consists of a peak at ~ 1.5 eV accompanied by a shoulder-like feature at ~ 1 eV. These features are well reproduced by numerical simulations

by assuming two peaks with a moderate background. This suggests the existence of a band splitting of ~ 0.5 eV at the K point in monolayer $1H$ -WTe₂.

It is emphasized here that the success of selective fabrication of $1H$ - and $1T'$ -WTe₂ is an important step to realize several exotic quantum phenomena as well as for device applications. Monolayer $1T'$ -WTe₂ would be used in 2D-TI-based devices where the band inversion and resultant spin current are controlled by an external electronic field. Monolayer $1H$ -WTe₂ is expected to serve as a useful platform to realize various exotic spin-valley-coupled phenomena such as the spin- or valley-Hall effect induced by circularly polarized light.⁶⁾ In addition, a lateral heterostructure consisting of $1T'$ - and $1H$ -WTe₂ would be used to generate chiral spin-currents at the topological edge by injecting spin-polarized carriers across the $1H$ - $1T'$ interface.

Acknowledgment

This work was supported by JST-CREST (no. JPMJCR18T1), JST-PRESTO (no. JPMJPR20A8), Grant-in-Aid for Scientific Research (JSPS KAKENHI Grant Numbers JP18H01821, JP20H01847, JP20H04624, JP21H01757, JP21K18888, JP21H04435, and JP22J13724), KEK-PF (Proposal No. 2020G669, 2021S2-001, and 2022G007), Foundation for Promotion of Material Science and Technology of Japan, Samco Foundation, and World Premier International Research Center, Advanced Institute for Materials Research. T. K. acknowledge support from GP-Spin at Tohoku University. T. K. also acknowledges support from JSPS.

*E-mail: k.sugawara@arpes.phys.tohoku.ac.jp, and t-sato@arpes.phys.tohoku.ac.jp

- 1) M. Chhowalla, H. S. Shin, G. Eda, L.-J. Li, K. P. Loh and H. Zhang, Nat. Chem., **5**, 263 (2013).
- 2) S. Cho, S. Kim, J. H. Kim, J. Zhao, J. Seok, D. H. Keum, J. Baik, D. -H. Choe, K. J. Chang, K. Suenaga, S. W. Kim, Y. H. Lee and H. Yang, Science, **349**, 625 (2015).
- 3) J. A. Champion, Br. J. Appl. Phys. **16**, 1035 (1965).
- 4) B. E. Brown, Acta. Crystallogr. **20**, 268 (1966).
- 5) C.-H. Lee, E. C. Silva, L. Calderin, M. A. T. Nguyen, M. J. Hollander, B. Bersch, T. E. Mallouk, and J. A. Robinson, Sci. Rep. **5**, 10013 (2015).
- 6) D. Xiao, G.-B. Liu, W. Feng, X. Xu, and W. Yao, Phys. Rev. Lett. **108**, 196802 (2012).
- 7) H. Zeng, J. Dai, W. Yao, D. Xiao, and X. Cui, Nat. Nanotech. **7**, 490 (2012).
- 8) D. Costanzo, S. Jo, H. Berger, and A. F. Morpurgo, Nat. Nanotechnol. **11**, 339 (2016).

- 9) A. A. Soluyanov, D. Gresch, Z. Wang, Q. S. Wu, M. Troyer, X. Dai, and B. A. Bernevig, *Nature* **527**, 495 (2015).
- 10) P. Li, Y. Wen, X. He, Q. Zhang, C. Xia, Z.-M. Yu, S. A. Yang, Z. Zhu, H. N. Alshareef, and X.-X. Zhang, *Nat. Commun.* **8**, 2150 (2017).
- 11) X. Qian, J. Liu, L. Fu, and J. Li, *Science* **346**, 6215 (2014).
- 12) P. Chen, W. W. Pai, Y.-H. Chan, W.-L. Sun, C.-Z. Xu, D.-S. Lin, M. Y. Chou, A.-V. Fedorov, and T.-C. Chiang, *Nat. Commun.* **9**, 2003 (2018).
- 13) L. Peng, Y. Yuan, G. Li, X. Yang, J. -J. Xian, C. -J. Yi, Y. -G. Shi, and Y. -S. Fu, *Nat. Commun.* **8**, 659 (2017).
- 14) K. Sugawara, T. Sato, Y. Tanaka, S. Souma, and T. Takahashi, *Appl. Phys. Lett.* **107**, 071601 (2015).
- 15) S. Tang, C. Zhang, D. Wong, Z. Pedramrazi, H. Tsai, C. Jia, B. Moritz, M. Claassen, H. Ryu, S. Kahn, J. Jiang, H. Yan, M. Hashimoto, D. Lu, R. G. Moore, C. Hwang, C. Hwang, Z. Hussain, Y. Chen, M. M. Ugeda, Z. Liu, X. Xie, T. P. Devereaux, M. F. Crommie, S. Mo, and Z. Shen, *Nat. Phys.* **13**, 683 (2017).
- 16) R. Ando, K. Sugawara, T. Kawakami, T. Takahashi, and T. Sato, *in preparation*
- 17) P. Giannozzi, S. Baroni, N. Bonini, M. Calandra, R. Car, C. Cavazzoni, D. Ceresoli, G. L. Chiarotti, M. Cococcioni, I. Dabo, A. D. Corso, S. de Gironcoli, S. Fabris, G. Fratesi, R. Gebauer, U. Gerstmann, C. Gougoussis, A. Kokalj, M. Lazzeri, L. Martin-Samos, N. Marzari, F. Mauri, R. Mazzarello, S. Paolini, A. Pasquarello, L. Paulatto, C. Sbraccia, S. Scandolo, G. Sclauzero, A. P. Seitsonen, A. Smogunov, P. Umari, and R. M. Wentzcovitch, *J. Phys. Condens. Matter* **21**, 395502 (2009).
- 18) J. P. Perdew, K. Burke, and M. Ernzerhof, *Phys. Rev. Lett.* **77**, 3865 (1996).
- 19) T. Kawakami, K. Sugawara, T. Kato, T. Taguchi, S. Souma, T. Takahashi, and T. Sato, *Phys. Rev. B* **104**, 045136 (2021).

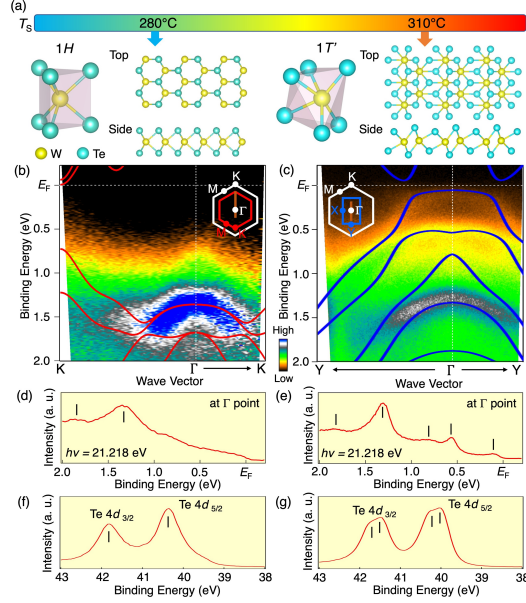


FIG. 1 (Color online). (a) Schematics of selective fabrication of $1H$ - and $1T'$ - WTe_2 monolayers by controlling the substrate temperature T_s . (b), (c) ARPES intensity plotted as a function of wave vector and binding energy for $1H$ - and $1T'$ - WTe_2 monolayers, respectively, measured along the ΓK cut of graphene BZ with $h\nu = 21.218$ eV. Inset shows the first BZ of graphene (white line), $1H$ - (red line), and $1T'$ - (blue line) WTe_2 . Corresponding DFT calculations for free-standing WTe_2 are overlaid for comparison. Calculations for $1H$ and $1T'$ phases were carried out with GGA and HSE06, respectively. (d), (e) EDC at the Γ point for $1H$ - and $1T'$ - WTe_2 , respectively. (f), (g) Te $4d$ core-level spectrum for $1H$ - and $1T'$ - WTe_2 , respectively, measured at $T = 40$ K with $h\nu = 80$ eV. Peak positions are marked by vertical lines. While the GGA calculation overall reproduces the experimental valence-band structure for both the $1H$ and $1T'$ phases, it was necessary to use HSE06 for the $1T'$ phase to reproduce the narrow band gap around E_F .

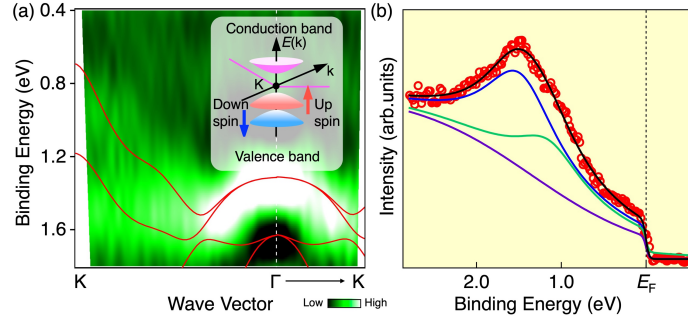


FIG. 2 (Color online). (a) Plot of second derivative intensity of ARPES spectrum for monolayer 1H-WTe₂, compared with the calculated band structure. Inset shows the schematic of spin-valley-coupled band structure around the K/K' point. (b) EDC at the K point and the result of numerical simulation (black curve) that assumes two Lorentzians (blue and green curves) with a moderate background (purple curve) multiplied by the Fermi-Dirac distribution function convoluted with the resolution function.